Low Temperature Heat Capacity of a Severely Deformed Metallic Glass

Jonas Bünz,[1*] Tobias Brink,[2] Koichi Tsuchiya,[3] Fanqiang Meng,[3] Gerhard Wilde,[1] and Karsten Albe[2]
[1]*Institut für Materialphysik, Westfälische Wilhelms-Universität Münster, Wilhelm-Klemm-Straße 10, D-48149 Münster, Germany*
[2]*Fachgebiet Materialmodellierung, Institut für Materialwissenschaft, TU Darmstadt, Jovanka-Bontschits-Straße 2, D-64287 Darmstadt, Germany*
[3]*National Institute of Materials Science, 1-2-1 Sengen, JP-305-0047 Tsukuba, Japan*
(Received 20 January 2014; published 1 April 2014)

The low temperature heat capacity of amorphous materials reveals a low-frequency enhancement (boson peak) of the vibrational density of states, as compared with the Debye law. By measuring the low-temperature heat capacity of a Zr-based bulk metallic glass relative to a crystalline reference state, we show that the heat capacity of the glass is strongly enhanced after severe plastic deformation by high-pressure torsion, while subsequent thermal annealing at elevated temperatures leads to a significant reduction. The detailed analysis of corresponding molecular dynamics simulations of an amorphous Zr-Cu glass shows that the change in heat capacity is primarily due to enhanced low-frequency modes within the shear band region.

DOI: 10.1103/PhysRevLett.112.135501 PACS numbers: 61.43.Dq, 61.43.Bn, 65.60.+a

Metallic glasses show mechanical, electrical, and magnetic properties, which can be very distinct from the properties of their crystalline counterparts [1]. One characteristic feature of glassy materials is a low-frequency enhancement of the vibrational density of states as compared with the Debye law. This excess contribution with respect to crystalline systems is commonly referred to as the boson peak. The boson peak is situated in the terahertz region of the vibrational spectrum and, hence, also influences the low temperature heat capacity. After several decades of controversy, it is now quite accepted that the boson peak is due to quasilocalized transverse vibrational modes associated with "defective" soft local structures in the glass [2–6]. The enhancement of the local vibrational density of states (often referred to as "soft modes") leads to additional scattering of phonons. The resulting contribution to the heat capacity c in excess of the Debye T^3 law becomes visible as a peak, if $c(T)/T^3$ is plotted in the temperature range of $T = 10$ to 40 K [7]. The boson peak is a general feature of glasses, irrespective of the dominant type of the interatomic or intermolecular binding energy and is, thus, also observed in metallic glasses. Although there is agreement concerning the connection between the phonon spectrum of glasses and the peculiarities of parts of the spectrum related to the boson-peak anomalies, the atomistic description of any structural origin of the low-frequency excited states remains unclear despite of numerous experimental and theoretical investigations. These excited states are described in terms of soft harmonic potentials [8,9], fluctuating force or elastic constants [10–14], strings of atoms [15], smeared out van Hove singularities [16,17], or interstitialcylike "defects" [18]. Even though the various models for describing the boson peak behavior differ in their specific assumptions and interpretations, they have in common that the glass state is described by spatially heterogeneously distributed regions having decreased elastic constants. These regions are distributed mesoscopically, i.e., on a scale of a few nanometers. In metallic glasses, rather localized and structurally disturbed regions occur upon application of external stress exceeding the elastic limit. These so-called shear bands have a typical thickness of the order of 10 nm [19] and present the regions where plastic shear strain was localized and quasiplastic straining occurred under the conditions of shear softening.

In order to analyze the contribution of shear bands to the low-temperature heat capacity, we performed measurements on a $Zr_{50}Cu_{40}Al_{10}$ metallic glass that was subjected to severe torsional deformation under a high applied hydrostatic pressure [20]. In a previous investigation of that material, individual shear bands could not be identified after applying large strain to the sample [20]. Nonetheless, the sample exhibits regions with deformation-induced structural changes, that can be considered as "macroscopic shear bands." Zr-based metallic glasses, especially the composition investigated here, show rather "strong" behavior concerning their fragility characteristics which, according to Ediger *et al.*, should lead to a more pronounced boson peak [21]. The sample was forced to withstand catastrophic failure by crack formation despite the large strain via geometrical confinement. In consequence, the regions of strong deformation localization, i.e., the shear bands, experienced severe conditions and the number of such regions is maximized [20].

Thus, this confined deformation up to severe strain values produces a specific state that is well suited to distinguish the contributions of shear band and matrix regions outside the shear bands. To that end, we performed molecular dynamics simulations of deformation of a $Cu_{64}Zr_{36}$ metallic glass—a model system comparable to

the Zr-Cu-Al glass—to differentiate the behavior of matrix and shear band regions in the glass.

Furthermore, we measured the response of the heat capacity at low temperatures upon the thermomechanical processing of the glass to gain more insights into the structural relaxation behavior of the deformed metallic glass.

The sample material, $Zr_{50}Cu_{40}Al_{10}$, was cast from ingots of pure metals to obtain an amorphous master ingot. We cut the master ingot into the specific dimensions for torsional deformation under an applied hydrostatic pressure (HPT). The HPT disks had a diameter of 10 mm, and a thickness of 0.89 mm. We deformed the samples with an applied pressure of 5 GPa for 50 revolutions. Further information about the materials processing can be found in Ref. [20].

The characteristic temperatures were measured by differential scanning calorimetry (DSC) experiments using a Perkin Elmer Diamond DSC. The experiments were performed with a constant heating rate of 20 K/ min under a high purity argon flow of 20 ml/ min.

We take the glass transition temperature T_g as the temperature where the increase of heat capacity during the glass transition amounts to half the value of the difference between the heat capacity of the liquid phase c_p^l and the glass phase c_p^g. We measured a glass transition temperature of 705 K and an onset of crystallization T_x at 769 K. The undercooled liquid interval accessible to calorimetry measurements at this heating rate amounts to $\Delta T = T_x - T_g = 64$ K.

The amorphicity of the samples was checked at room temperature by x-ray diffraction (XRD) with a Siemens D5000 diffractometer. The samples, both deformed and as cast, show identical broad diffraction maxima typical for the amorphous phase. There is no sign of partial crystallization, nor did the HPT deformation change the structure in a way detectable in XRD.

The heat capacity c_p was measured under high vacuum conditions with a Quantum Design Physical Property Measurement System, which allows cooling down to 2 K with a liquid helium system. The samples were polished for good thermal contact and cut into 2.5×2.5 mm^2 pieces, each with a mass of 10 to 20 mg. The samples were placed on top of a sapphire block of known heat capacity c_a with a thermal grease to ensure good thermal contact. At each temperature, a known heat pulse is applied and sample and platform are heated to a temperature $T_p(t)$. After the end of the heat pulse, the sample temperature relaxes to the heat sink temperature T_0 according to

$$T_p(t) = T_0 + \Delta T \exp(-t/\tau), \quad (1)$$

with the time constant $\tau = (c_p + c_a)/K$ [22]. The factor K is the thermal conductance between the sample platform and heat sink. The heat capacity c_p can now be measured by fitting the temperature decay τ with an accuracy better than 3%. Prior to the measurement of the samples, we measured K and c_a with an empty sapphire crystal with the applied grease for baseline correction.

Each heat capacity curve in this work includes three individual measurements at each temperature to ensure reproducibility. We chose the spacing between temperatures in a logarithmic way to preferentially sample the region of low temperature.

The annealing of the samples above 394 K was done in a TA Instruments Q500 DSC under constant argon flow of 50 ml/ min. Annealing at temperatures below 393 K and for long times was performed in a Thermometric TAM III microcalorimeter. Both methods allow us to simultaneously measure the emitted heat flow to investigate relaxational events and exclude crystallization. For obtaining a crystalline reference of identical composition, we heated a $Zr_{50}Cu_{40}Al_{10}$ sample up to 823 K, 60 K above the crystallization temperature.

Molecular dynamics (MD) computer simulations using the software LAMMPS [23] were used for discriminating the matrix and shear band contributions to the heat capacity. For this purpose, we simulated a $Cu_{64}Zr_{36}$ system using the Finnis-Sinclair type potential by Mendelev *et al.* [24]. A bulk metallic glass sample was prepared by quenching from the melt to 50 K with a cooling rate of 10^{10} K/s. The simulation box, consisting of 364 500 atoms, was generated by a $2 \times 2 \times 2$ replication of the quenched system. We induced shear band formation using a volume conserving pure shear deformation with a shear rate of 10^8 s^{-1} up to a maximum shear of 20%. Additionally, we annealed the deformed sample at 500 K for 20 and 40 ns.

We used the von Mises local shear invariant η_i [25] as implemented by OVITO [26] as a criterion for distinguishing atoms: Atoms with $\eta_i > 0.2$ were marked as belonging to the shear band or shear transformation zones, while all others were considered as matrix atoms.

As a first step to obtain heat capacity values, we calculated the phonon density of states (PDOS) from the Fourier-transform of the velocity autocorrelation function [27]. This was done separately for the atoms in the shear band and in the matrix after unloading and equilibrating the system with a barostat at zero stress.

To calculate the corresponding heat capacities from the phonon density of states $g(\omega)$, we employed the harmonic approximation of the free energy [28]

$$c(T) = k_B \int_0^\infty \left(\frac{\hbar\omega}{2k_BT}\right)^2 \sinh^{-2}\left(\frac{\hbar\omega}{2k_BT}\right) g(\omega) \mathrm{d}\omega. \quad (2)$$

In this model, we assume $c = c_V = c_p$, which gives a reasonable approximation at low temperatures. As a reference, we also calculated heat capacities for the CuZr $B2$ crystal using the same method.

Note that the direct calculation of the specific heat from the time averaged inner energy given by the classical trajectories in MD simulations would yield unphysical values in the low temperature regime due to the missing quantum-statistical contributions.

The experimentally measured heat capacity is plotted as $\Delta c_p/T^3$ versus T in Fig. 1(a), making visible the contribution of the boson peak at low temperatures. The c_p curve of the crystalline Zr-Cu-Al sample is used as a reference and, therefore, subtracted from the data of each amorphous sample. Since the crystalline sample shows no contribution to the boson peak but a comparable heat capacity from electronic and "lattice" contributions, the excess heat capacity plotted in Fig. 1(a) is solely due the boson peak.

The HPT-deformed glass shows an enhanced peak, whose height is almost twice as high compared to the as-cast state. The peak maximum of the deformed sample is slightly shifted by 2.7 K to lower temperatures.

We annealed the samples at different temperatures with simultaneous measurement of the relaxational heat flow in the microcalorimeter. After at most seven days, the heat flow signal reached the background, indicating that the sample was close to an equilibrium state at that temperature. The undeformed sample shows a slight decrease of the boson peak after annealing at 393 K, while annealing at 333 and 353 K lowers the boson peak of the deformed sample to an intermediate height between the deformed and the as-cast state. The deformation "defects" are not completely healed by the thermal treatment. Otherwise, the sample that was annealed at 393 K shows a boson peak which is even lower than the boson peak of the as-cast sample or of the undeformed sample relaxed at 393 K. Additional DSC experiments were performed and did not show any evidence for partial crystallization during annealing. Furthermore, we heated a HPT-deformed sample to 743 K $> T_g$. The sample reaches internal equilibrium within the first 10 s of annealing and has a defined thermal history after cooling with 20 K/ min. The boson peak has the same height as one of the HPT-deformed samples which is in metastable equilibrium at 393 K. The undeformed sample, which was equilibrated at the same temperature, shows a 20% higher boson peak.

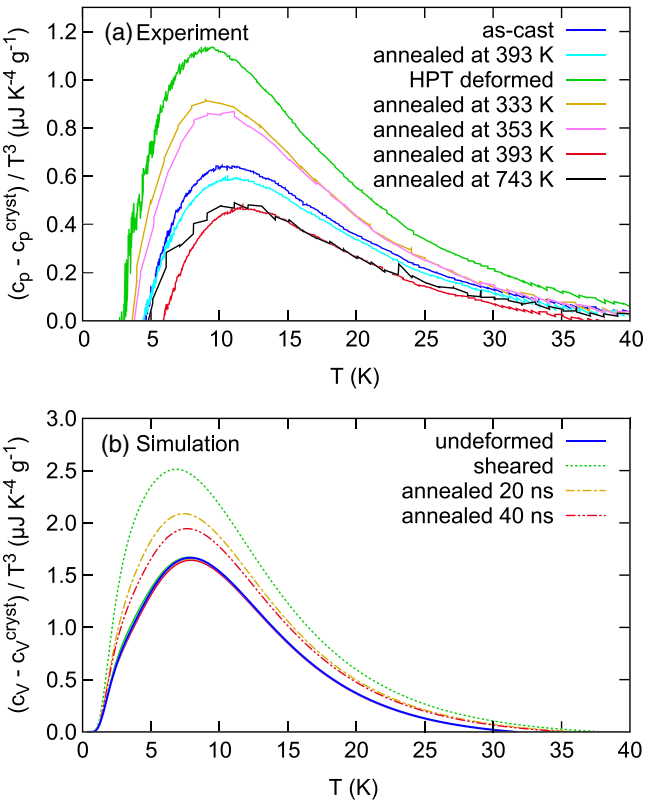

FIG. 1 (color online). Difference in heat capacity between glass and crystal. (a) Experimental data, annealing below 393 K was done for one week, annealing at 743 K for 10 s. (b) Simulation data, dashed lines are data from shear bands, solid lines from the rest of the sample.

In Fig. 2, the PDOS calculated by the computer simulation is shown. The data are split into contributions of the matrix (solid lines) and contributions of the shear band (dashed lines). The data is plotted for the as-quenched glass, the glass deformed to a shear of 20%, and the deformed sample annealed for 20 and 40 ns at 500 K. Most evidently, the vibrational spectrum of the matrix does not change between the undeformed, sheared, and annealed samples, whereas the spectrum of the shear band shows an increased boson peak which reduces again with annealing. Figure 1(b) shows the corresponding heat capacities c_V calculated from the PDOS. As in the experiment—and as already suggested by the PDOS—the boson peak in the heat capacity increases after deformation and decreases again after annealing. The simulation overestimates the difference in heat capacity between crystal and glass but shows qualitatively the same features as the experiment. Because of the small time scale accessible by the simulation, we don't observe a complete recovery of the shear band in the deformed glass by thermal annealing.

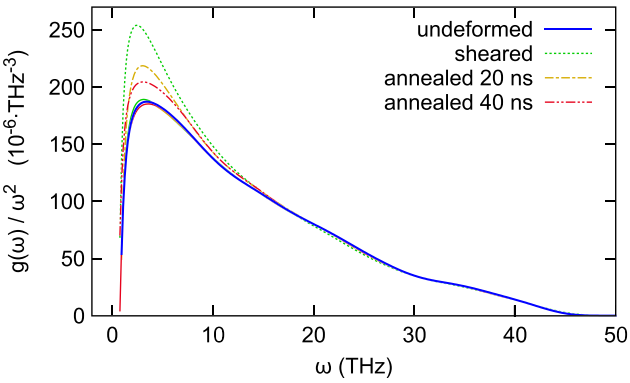

FIG. 2 (color online). Phonon density of states from computer simulation. Dashed lines are data from shear bands, solid lines from the rest of the sample.

However, the computer simulations clearly show that the shear band regions relax to a state of lower excess heat capacity, while the contribution of the matrix is not changing. The experimentally observed fact that the deformed sample shows a significantly reduced boson peak after thermal annealing at high temperature as compared to the as-cast case is indicative of a structural relaxation. Since the excess with respect to the crystalline reference is reduced, this suggests a relaxation towards a more crystal-like state within the shear band region. This interpretation is supported by recent results indicating the prevalence of shear bands for the formation of nanocrystals or crystal-like medium range order [19,29]. The enhanced atomic mobility within the shear bands [30] does also favor the relaxation of the modified glass structure towards a more ordered state.

The change of the boson peak with applied pressure can often be explained by mere changes of the elastic constants. In these cases, the change of the peak height is accompanied by a shift of the boson-peak frequency. When plotting the data in units of the Debye frequency, the peaks collapse to one curve [12,17]. In our case, the frequency of the boson peak, and therefore its position in the heat capacity plot, does not shift in either experiment or simulation. This indicates a real change of the disorder statistics, i.e., the distribution of local moduli, and not only a change of the global elasticity.

All in all, our findings clearly show that all changes of the specific heat induced by plastic deformation and annealing stem from the regions of strain localization. The matrix will stay relatively intact in the processes.

Both experimental and simulation data show that plastic deformation enhances the boson contribution to the heat capacity. Molecular dynamics simulations provide direct evidence that the additional contributions to the boson peak result from structures that are located in the shear bands, while the PDOS in the matrix stays unchanged with deformation and annealing. The experiment supports this perspective as the change of boson peak height of the undeformed samples during annealing is relatively small compared to the deformed samples.

It should be noted that in our current work the experimental conditions always lead to a strong strain localization. The analysis given here does not cover a more homogeneous deformation behavior, in which the matrix could also show a changed vibrational spectrum, if there is even a distinction between shear band and matrix. In this case, an increase of the boson peak after deformation may be observed over the whole system.

Several studies show that shear bands can heal during annealing even at temperatures well below T_g [31–33]. In contrast, our findings indicate that the shear band structure after annealing differs from an annealed, undeformed glass. Diffusion studies demonstrate accelerated diffusion [30] and excess free volume [34] inside of shear bands. This could promote structural relaxation and short to medium range ordering that drives the system to another metabasin in the energy landscape [35]. This metabasin would exhibit different structural properties: The decrease of the boson peak below the values of the undeformed glass in that case suggests an increasingly crystal-like structure.

The authors thank Yoshihiko Yokayama (Institute of Metal Research, Tohoku University) for providing the amorphous ingot material and Leonie Koch for providing the model structures. The authors gratefully acknowledge the computing time granted by the John von Neumann Institute for Computing (NIC) and provided on the supercomputer JUROPA at Jülich Supercomputing Centre (JSC). Financial support by DFG Grants No. Al-578/13-1 and No. WI-1899/12-1 is gratefully acknowledged. This work is partly supported by the Grant-in-Aid for Scientific Research on Innovative Area "Bulk Nanostructured Metals" through MEXT, Japan (Contract No. 22102004).

*jonasbuenz@uni-muenster.de

[1] W. H. Wang, C. Dong, and C. H. Shek, Mater. Sci. Eng. R **44**, 45 (2004).
[2] H. Shintani and H. Tanaka, Nat. Mater. **7**, 870 (2008).
[3] H. R. Schober, J. Non-Cryst. Solids **357**, 501 (2011).
[4] H. R. Schober and B. B. Laird, Phys. Rev. B **44**, 6746 (1991).
[5] B. B. Laird and H. R. Schober, Phys. Rev. Lett. **66**, 636 (1991).
[6] P. M. Derlet, R. Maaß, and J. F. Löffler, Eur. Phys. J. B **85**, 1 (2012).
[7] C. A. Angell, Science **267**, 1924 (1995).
[8] V. G. Karpov, M. I. Klinger, and F. N. Ignat'ev , Zh. Eksp. Teor. Fiz. **84**, 760 (1983).
[9] L. Gil, M. A. Ramos, A. Bringer, and U. Buchenau, Phys. Rev. Lett. **70**, 182 (1993).
[10] W. Schirmacher and M. Wagener, Solid State Commun. **86**, 597 (1993).
[11] W. Schirmacher, G. Diezemann, and C. Ganter, Phys. Rev. Lett. **81**, 136 (1998).
[12] W. Schirmacher, Europhys. Lett. **73**, 892 (2006).
[13] W. Schirmacher, G. Ruocco, and T. Scopigno, Phys. Rev. Lett. **98**, 025501 (2007).
[14] C. Ferrante, W. Pontecorvo, G. Cerullo, A. Chiasera, G. Ruocco, W. Schirmacher, and T. Scopigno, Nat. Commun. **4**, 1793 (2013).
[15] H. R. Schober and C. Oligschleger, Phys. Rev. B **53**, 11469 (1996).
[16] S. N. Taraskin, Y. L. Loh, G. Natarajan, and S. R. Elliott, Phys. Rev. Lett. **86**, 1255 (2001).
[17] A. I. Chumakov, G. Monaco, A. Monaco, W. A. Crichton, A. Bosak, R. Rüffer, A. Meyer, F. Kargl, L. Comez, D. Fioretto, H. Giefers, S. Roitsch, G. Wortmann, M. H. Manghnani, A. Hushur, Q. Williams, J. Balogh, K. Parliński, P. Jochym, and P. Piekarz, Phys. Rev. Lett. **106**, 225501 (2011).
[18] A. N. Vasiliev, T. N. Voloshok, A. V. Granato, D. M. Joncich, Y. P. Mitrofanov, and V. A. Khonik, Phys. Rev. B **80**, 172102 (2009).

[19] G. Wilde and H. Rösner, Appl. Phys. Lett. **98**, 251904 (2011).
[20] F. Meng, K. Tsuchiya, S. II, and Y. Yokoyama, Appl. Phys. Lett. **101**, 121914 (2012).
[21] M. D. Ediger, C. A. Angell, and S. R. Nagel, J. Phys. Chem. **100**, 13200 (1996).
[22] J. C. Lashley, M. F. Hundley, A. Migliori, J. L. Sarrao, P. G. Pagliuso, T. W. Darling, M. Jaime, J. C. Cooley, W. L. Hults, L. Morales, D. J. Thoma, J. L. Smith, J. Boerio-Goates, B. F. Woodfield, G. R. Stewart, R. A. Fisher, and N. E. Phillips, Cryogenics **43**, 369 (2003).
[23] S. Plimpton, J. Comput. Phys. **117**, 1 (1995).
[24] M. I. Mendelev, M. J. Kramer, R. T. Ott, D. J. Sordelet, D. Yagodin, and P. Popel, Philos. Mag. **89**, 967 (2009).
[25] F. Shimizu, S. Ogata, and J. Li, Mater. Trans. **48**, 2923 (2007).
[26] A. Stukowski, Model. Simul. Mater. Sci. Eng. **18**, 015012 (2010); http://ovito.org/.
[27] J. M. Dickey and A. Paskin, Phys. Rev. **188**, 1407 (1969).
[28] R. K. Pathria, *Statistical Mechanics* (Elsevier Butterworth-Heinemann, Oxford, 1996), 2nd ed.
[29] H. Rösner, C. Kübel, M. Peterlechner, and G. Wilde, Ultramicroscopy (to be published).
[30] J. Bokeloh, S. V. Divinski, G. Reglitz, and G. Wilde, Phys. Rev. Lett. **107**, 235503 (2011).
[31] W. H. Jiang, F. E. Pinkerton, and M. Atzmon, Acta Mater. **53**, 3469 (2005).
[32] S. Xie and E. P. George, Acta Mater. **56**, 5202 (2008).
[33] Y. Ritter and K. Albe, Acta Mater. **59**, 7082 (2011).
[34] B. P. Kanungo, S. C. Glade, P. Asoka-Kumar, and K. M. Flores, Intermetallics **12**, 1073 (2004).
[35] A. Heuer, J. Phys. Condens. Matter **20**, 373101 (2008).